In situ electrostatic characterisation of ion beams in the region of ion acceleration

Alexander Bennet, Christine Charles, and Rod Boswell

Citation: Physics of Plasmas **25**, 023516 (2018); doi: 10.1063/1.5017049
View online: https://doi.org/10.1063/1.5017049
View Table of Contents: http://aip.scitation.org/toc/php/25/2
Published by the American Institute of Physics

In situ electrostatic characterisation of ion beams in the region of ion acceleration

Alexander Bennet,[a] Christine Charles, and Rod Boswell
Space Plasma, Power and Propulsion Laboratory, Research School of Physics and Engineering, The Australian National University, Canberra, ACT 2601, Australia

(Received 23 November 2017; accepted 7 February 2018; published online 26 February 2018)

In situ and *ex situ* techniques have been used to measure directional ion beams created by a sharp axial potential drop in low pressure expanding plasmas. Although Retarding Field Energy Analysers (RFEAs) are the most convenient technique to measure the ion velocities and plasma potentials along with the plasma density, they are bulky and are contained in a grounded shield that may perturb the electric potential profile of the expanding plasma. In principle, *ex situ* techniques produce a more reliable measurement and Laser Induced Fluorescence spectroscopy (LIF) has previously been used to characterise the spatial velocity profile of ion beams in the same region of acceleration for a range of pressures. Here, satisfactory agreement between the ion velocity profiles measured by LIF and RFEA techniques has allowed the RFEA method to be confidently used to probe the ion beam characteristics in the regions of high gradients in plasma density and DC electric fields which have previously proven difficult. *Published by AIP Publishing.*
https://doi.org/10.1063/1.5017049

I. INTRODUCTION

Radio-frequency (RF), electrodeless, neutraliser-free plasma thrusters are of interest to the electric propulsion community as they can provide extended lifetimes and power scaling, and reduce the complexity of subsystems through the removal of neutralisers compared to mature technologies like Hall effect and gridded ion thrusters.[1,2] Helicon thrusters like the Helicon Double Layer Thruster (HDLT) fall within this category of RF, electrodeless, neutraliser-free devices and are the subject of a wide body of ongoing research, e.g., Refs. 3–5. The HDLT generates thrust by creating a high density plasma and accelerates this through a magnetic nozzle coincident with the geometric expansion at the outlet of the thruster.[6] At sufficiently low pressures, the combination of a diverging magnetic field and geometric expansion spontaneously forms a strong, thin ambipolar electric field and corresponding plasma potential structure known as a double layer, accelerating ions away from the thruster.[7] Many experimental plasma devices have shown the existence of double layers and double layer-like potential structures[8–11] and have been used to study areas like thruster performance,[12–14] plasma transport,[15–17] and thermodynamics of expanding plasmas,[18] to name a few. Key to many of these studies is the ability to measure various plasma characteristics like plasma potential, ion beam energy, and electron temperature inside the plasma source region where high density plasma and strong RF electric fields are present. The use of electrostatic probes to directly measure plasma parameters is common; however, these are known to be perturbative to varying degrees, depending on the size and material of the probe. Non-perturbative techniques like laser induced fluorescence spectroscopy (LIF) have also been used to characterise expanding plasmas;[19–22] however, these make assumptions about ion metastable states and their ability to represent the entire ion population. Still, LIF studies have previously shown the technique's ability to detect and measure the energy and velocity of the ion beam created by double layers in multiple devices.[20,23] The measurement of beam energy is particularly important to understanding thrusters like the HDLT as the ion beam accounts for the main thrust mechanism. As such, understanding the limitations and applications of these measurement techniques is crucial. A number of studies have previously compared ion velocity distribution functions (IVDFs) measured using LIF and retarding field energy analyser (RFEA) techniques downstream of plasma sources,[24,25] with Ref. 26 presenting a comprehensive analysis in this region. The focus of the present study is to determine the ability of intrusive, *in situ* retarding field energy analysers (RFEAs) to measure ion beam velocities and densities in regions of high RF and DC electric fields, i.e., in the source and double-layer regions of expanding plasma devices, by first comparing with previous work done with non-perturbative LIF techniques to assess the technique's validity.

II. PREVIOUS LIF MEASUREMENTS IN CHI KUNG

The general theory of LIF measurements has been published extensively. As such, the focus here is on previous experiments in expanding plasma devices and, in particular, the study conducted by Keesee *et al.* in Ref. 23. The experiments in the study used a portable, tunable-diode-laser system to take LIF measurements in the Chi Kung helicon plasma reactor at the Australian National University, shown in Fig. 1. The laser, tuned to 668.6138 nm and aligned on the central axis of the reactor, was used to pump argon ions in the metastable 3d $^4F_{7/2}$ state to the 4p $^4D_{5/2}$ state while

[a]Email: alex.bennet@anu.edu.au

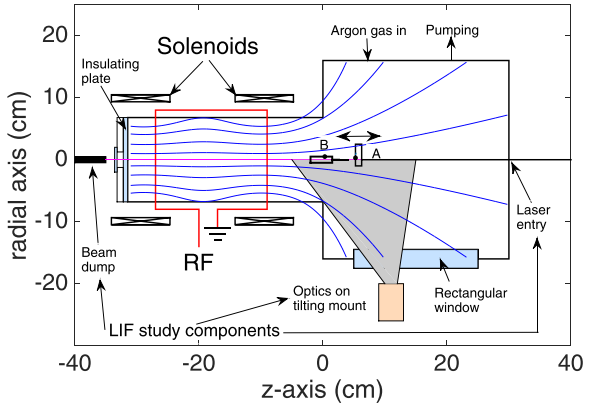

FIG. 1. Schematic of the Chi Kung plasma reactor showing the helicon source and expansion chamber, RF antenna, solenoids and magnetic field lines (blue solid lines), gas input location, and pumping location. Also plotted for comparison are the main components of the LIF study previously conducted by Keesee *et al.* in Ref. 23, comprising of a laser beam entering through the faceplate of the diffusion chamber, a beam dump at the closed end of the source to minimise beam reflection, and optics set up on an external tilting mount; the maximum axial range of LIF investigation is $-5\ \text{cm} \leq z \leq 15\ \text{cm}$. RFEAs in either source-facing (A) or radial-facing (B) configurations can be moved axially through the entire chamber.

measuring the fluorescent radiation emitted at 442.7244 nm as ions decay from this state to the 4s $^4P_{3/2}$ state. The Doppler shift of the emitted radiation yields the velocity of the 3d $^4F_{7/2}$ metastable ion species and assumes this is representative of the total accelerated ion population. The fluorescent radiation was measured with optics supported on a tilting mount outside the vacuum chamber, accessing the radiation via a rectangular window. Major components of the LIF setup used in Ref. 23 can be seen in Fig. 1. The tilting mount used limited the range of axial measurements to −5 cm to 25 cm and the optics allowed for spatial resolution of approximately 1 cm. The laser used in these experiments was of relatively low power, and combining this with low plasma densities required RF powers greater than 400 W and long measurement times (5 min per measurement), a factor which limited the RF power to a maximum of about 750 W as heating of the system components became a limitation. In this study, Keesee *et al.* measured the ion velocities in the region of the double layer-like potential structure and showed how the velocities evolved through the ambipolar electric field for two different pressures of neutral argon gas, 0.37 and 0.55 mTorr. The axial velocity profile showed a region of rapidly increasing ion velocity, relating to the location and width of the double layer and presheath, followed by a plateau region in the diffusion chamber downstream of the double layer as the region of significant ion acceleration had passed. In the same year, many of the same authors also showed that this technique could be optimised, overcoming the limitations of the Chi Kung test campaign; the axial beam energy throughout the entire HELIX expanding plasma device was mapped to show how the beam energy evolves through the potential drop in Ref. 21.

Using the results of Ref. 23, the present study aims to compare the use of RFEAs through the potential drop in the Chi Kung reactor with the LIF results in the region of ion acceleration a decade after the original LIF campaign, determining an RFEA's suitability for ion velocity and density measurement in this region and potentially validating the results of the LIF study in much greater detail.

III. CHI KUNG EXPERIMENTAL SETUP

To compare with Ref. 23, the experiments in this study have been conducted in the Chi Kung plasma reactor. Described in detail previously[27] and shown in Fig. 1, Chi Kung consists of a 31 cm long, 0.65 cm thick, 13.7 cm inner diameter Pyrex plasma source tube contiguously connected to a 30 cm long, 32 cm inner diameter grounded aluminium expansion chamber. The coordinate system used in the present study defines the interface between the plasma source and diffusion chamber as z = 0 cm. The end of the source tube furthest from the expansion chamber is terminated by a circular glass plate which ensures that all walls of the source region are floating. The aluminium expansion chamber is terminated by an aluminium plate fitted with feedthroughs available for diagnostic probes. Two solenoids in a Helmholtz pair configuration are centred on z = −9 cm and z = −28.6 cm and, when fed with equal current, can provide a near-parallel magnetic field in the source region and a diverging field in the expansion chamber. In this study, 6 A of DC current is supplied to the solenoids, creating a maximum axial magnetic field of about 145 G which then drops to a few tens of gauss in the expansion chamber. Surrounding the source tube and centred on z = −18 cm is an 18 cm long double saddle antenna fed with radio-frequency (RF) power at 13.56 MHz from an ENI generator and L-matching circuit. A pumping system consisting of turbomolecular and rotary pumps maintains a base chamber pressure of 2 to 4×10^{-6} Torr. Gas is introduced into the system through a side port in the expansion chamber at z = 7 cm.

IV. DIAGNOSTICS

The data have been taken with a retarding field energy analyser (RFEA) in ion collection mode, the design of which has been described in detail previously[28] and used in several studies in the Chi Kung reactor.[7,27,29] The RFEA allows ions over a certain energy to reach a collecting electrode by sweeping a discriminator voltage, V_D, from 0 to 80 V. Electrons entering the analyser are firstly repelled by the surrounding sheath and again by a repellor grid biased to −80 V while secondary electrons possibly generated at the collector due to bombarding ions are not permitted to leave the collector due to a negatively biased grid. Because ions can only enter the analyser through an orifice on one side of its housing, the measured ion current is directional (within an acceptance solid angle of ∼40°).

Previous studies have used source-facing RFEAs in the expansion chamber to measure both accelerated and local ion populations and characterise a beam formed from double layers and double layer-like DC axial electric potential structures. Radial-facing RFEAs can be used to only measure the characteristics of the local ion population which is created by a combination of ionisation and ion-neutral charge exchange collisions between beam ions exiting the source

and neutral gas present downstream.[30] The ion energy distribution function (IEDF) of ions that have fallen through the sheath of the grounded probe is proportional to the first derivative of the probe's I-V trace[29] and generally appears as a Gaussian distribution centred around the plasma potential. Radial-facing RFEAs have been used previously to measure the plasma potential and density in both the source and expansion chambers of Chi Kung.[29] For source-facing RFEA measurements in the presence of an ion beam, two Gaussian distributions are detected: the local population centred around the plasma potential, V_p, and a beam population centred around a "beam potential," V_b, with the latter typically corresponding to the maximum upstream plasma potential. To illustrate this, the normalised first derivatives of current detected by the RFEA, dI/dV_D, measured at the same axial location ($z = 0$ cm), a pressure of 0.3 mTorr, and 315 W RF power are shown in Fig. 2 for both source-facing and radial-facing RFEAs. In the radial-facing case, the first derivative exhibits a single peak, representing the local population of ions with a potential of about 38 ± 0.4 V. The ion populations measured by the source-facing RFEA shows two peaks: the first corresponding to the local population as found by the radial-facing RFEA and a higher energy population at about 53.8 ± 0.4 V. The latter is identified as a $\sim$15.8 eV directional ion beam flowing in the +z direction as it only exists in the source-facing measurements. This method of identifying and characterising ion beams has been used extensively in studies that use ion energy analysers and has allowed for the downstream characterisation of plasma and beam behaviour.

A. Density measurement techniques

RFEA studies infrequently present absolute values of plasma density, with authors opting to show the measured ion currents of local and beam populations due to difficulties associated with RF broadening of the measured distribution and the plasma potential drop around the large, grounded

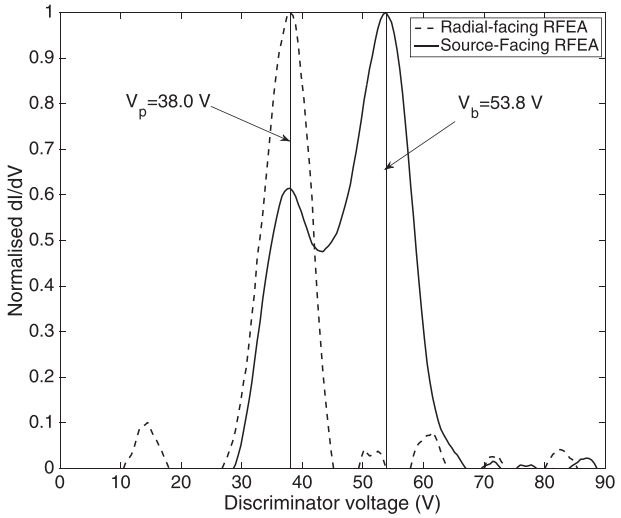

FIG. 2. Normalised derivatives of the RFEA I-V curve, dI/dV_D for source-facing (solid line) and radial-facing (dashed line) RFEAs located at $z = 0$ cm for a pressure of 0.3 mTorr and 315 W of RF power and a maximum axial magnetic field of $\sim$145 G.

probe.[26] Furthermore, because the I-V curve measured by the RFEA is a current measurement in energy space, the measurement is particularly susceptible to the ion flow speed entering the grounded probe. This means that it is not trivial to calibrate the current measurement to an absolute density in an experiment like Chi Kung in which the plasma potential and electron temperature vary spatially. Additional analysis is also required to characterise the beam density as the high ion velocity will artificially increase the measured beam current. Previous studies have accounted for the effect of ion velocity on the measured current by either fitting the raw RFEA I-V trace to integrated drifting Maxwellian distributions[24,25] or fitting Gaussian distribution functions to the derivative of the I-V trace and considering the ion flux entering the sheath around the RFEA.[27]

1. Drifting Maxwellians method

The current measured by an RFEA due to a single stationary Maxwellian population that has been accelerated through the surrounding sheath is given by the following equation:[24]

$$I(V_D) = \sqrt{\frac{(n/2)^2 q^2}{2M_{Ar}\pi}}\left[\sqrt{T}e^{-\left((\sqrt{qV_D}-\sqrt{E})^2/T\right)} + \sqrt{E\pi}\,\mathrm{erfc}\left[\left(\sqrt{eV_D}-\sqrt{E}\right)/\sqrt{T}\right]\right]. \quad (1)$$

$I(V_D)$ is the current measured by the collecting electrode as a function of the discriminator voltage V_D, n is the ion density of the population, T is the temperature of the ion population, and E is the energy of the drifting population as it enters the RFEA, i.e., for a stationary population, the energy of the drifting population is equal to qV_p because the population is accelerated by the sheath surrounding the grounded probe. The $n/2$ term is included for isotropic, stationary plasmas as only half of the local distribution travelling towards the probe is measured.[24]

For a bimodal ion population in which a beam and a local population exist, the ion current can be described by the sum of two drifting Maxwellian populations,

$$I(V_D) = \sqrt{\frac{q^2}{2M_{Ar}\pi}}\left[\frac{n_{loc}}{2}\left(\sqrt{T_{loc}}e^{-\left((\sqrt{qV_D}-\sqrt{E_{loc}})^2/T_{loc}\right)} + \sqrt{E_{loc}\pi}\,\mathrm{erfc}\left[\left(\sqrt{eV_D}-\sqrt{E_{loc}}\right)/\sqrt{T_{loc}}\right]\right) + n_b\left(\sqrt{T_b}e^{-\left((\sqrt{qV_D}-\sqrt{E_b})^2/T_b\right)} + \sqrt{E_b\pi}\,\mathrm{erfc}\left[\left(\sqrt{eV_D}-\sqrt{E_b}\right)/\sqrt{T_b}\right]\right)\right], \quad (2)$$

where the subscripts "loc" and "b" refer to the local and beam populations, respectively, and $E_{loc} = qV_p$, $E_b = qV_b$. These integrated distributions can be fit to the raw RFEA I-V data, yielding the values of the distribution parameters. This method treats the energy of an incident ion population separately to its density, and the calibration of the density measurement can therefore be treated independently of the

velocity. Calibration with a Langmuir probe using Sheridan's analysis[31,32] at a stationary location in the plasma (z = −25 cm) must still be undertaken because the current measurement has not been adjusted for effects like the transmission factor of the biased grids or the acceptance angle of the RFEA, for example; however, these effects are assumed to be consistent across measurements with the same RFEA and can be accounted for through calibration. For a radial-facing RFEA, only one population of ions is expected and (1) can be used, whereas the source facing RFEA exhibits a bimodal population and therefore (2) must be used.

2. Gaussian-flux method

The derivative of the RFEA I-V curve for a single ion population can be fitted with a simple Gaussian of the form

$$f(V_D) = ae^{-\left(\frac{V_D - V_p}{c}\right)^2}, \tag{3}$$

where a and c are fitting parameters. The total ion current, $I(0)$, measured by the RFEA is equivalent to the integral of $f(V_D)$,

$$I(0) = \int_{-\infty}^{\infty} f(V_D) = ac\sqrt{\pi}. \tag{4}$$

The measured ion current is a function of both ion density and velocity and can therefore be related to the flux of particles entering the sheath of the RFEA by noting that a stationary plasma at position z will enter the sheath at the ion sound speed, $c_{s,z} = \sqrt{kT_{e,z}/M_{Ar}}$,

$$I_z(0) = qAT^4 n_z c_{s,z}. \tag{5}$$

Using the density measurement found with the Langmuir probe through Sheridan's analysis at z = −25 cm, the current due to a flux of ions incident on the probe can be calibrated.[27] Using this calibration and a radial facing RFEA, the local density can be found anywhere on axis using

$$\begin{aligned} \frac{I_z}{I_{-25}} &= \frac{n_z c_{s,z}}{n_{-25} c_{s,-25}}, \\ n_z &= \frac{I_z n_{-25} c_{s,-25}}{I_{-25} c_{s,z}}. \end{aligned} \tag{6}$$

Equation (6) shows that knowledge of the local electron temperature is required through the ion sound speed terms.

For a plasma containing an ion beam measured with a source-facing RFEA, one Gaussian centred on V_p can be fit to the local population and another centred on V_b can be fit to the beam population

$$f(V_D) = \frac{a_1}{2} e^{-\left(\frac{V_D - V_p}{c_1}\right)^2} + a_2 e^{-\left(\frac{V_D - V_b}{c_2}\right)^2}, \tag{7}$$

where the $a_1/2$ is included because the local population is treated in the same manner as in the drifting Maxwellians method. Following from Eq. (7), the current detected by the RFEA for each population can be found from these fits

$$I_{loc} = a_1 c_1 \sqrt{\pi}; \quad I_b = a_2 c_2 \sqrt{\pi}. \tag{8}$$

If the local density is known, the ratio I_b/I_{loc} can be related to the population fluxes in a similar manner to the local density calibration method described earlier,

$$n_b = \frac{I_b n_{loc} c_{s,loc}}{I_{loc} v_b}. \tag{9}$$

The authors of Ref. 24 noted that the ion temperature predicted by the drifting Maxwellians method is overestimated due to RF broadening of the RFEA I-V curve, an effect discussed in Ref. 33. As such, any RF broadening is largely coupled with the temperature parameter, not the density. For the Gaussian-flux method, the integral used to determine the ion current associated with each population incorporates any RF broadening and may result in overestimation of the density. At the power and RF frequency used in this paper, the ion density is low (10^9 to low 10^{11} cm^{-3}, see later) and the RF signal is not expected to cause large ion transit time broadening of the I-V characteristics measured by the RFEA; however, this could be characterised somewhat by comparing the two methods of density calculation.

This study uses both source-facing and radial-facing RFEAs to investigate the plasma potential and density along Chi Kung's main axis with increasing gas pressures for comparison with the results from LIF at the source-chamber interface region and investigation of the beam velocity and density. Both methods for density characterisation described here are used to determine the axial plasma and beam density and the results compared.

V. PLASMA POTENTIAL, DENSITY, AND BEAM DETECTION MEASUREMENTS

Argon gas is introduced to the system at pressures ranging from 0.3 mTorr to 0.7 mTorr in increments of 0.1 mTorr while a pressure of 2 mTorr was also investigated as a high pressure limit. It has been noted previously that a potential decrease near z = −5 cm results in axial ion acceleration, leading to supersonic ion velocities in the +z direction in the expansion chamber.[7,23] Previous studies have also shown that this accelerated population of beam ions disappears at pressures >1–2 mTorr as the source potential decreases due to increase in collision rates.

For this study, 315 W of RF power is supplied to the RF antenna and generates an inductively coupled plasma in the source region. For the pressures under investigation, the ion-neutral mean free path is in the range $\lambda_i \sim$ 1–8 cm, which is comparable to the source tube diameter for the lower pressures tested. Figure 3(a) shows the axial plasma potential profiles measured by the radial-facing RFEA for increasing pressures. The results show that over the axial region from z ≈ −10 – 0 cm, the plasma potential decreases rapidly, creating a DC axial electric field accelerating ions into the expansion chamber as the plasma expands through the throat of the magnetic nozzle. The location of the potential drop can also be seen to move further downstream as the pressure increases, consistent with the LIF measurements in Ref. 23. To illustrate why this is, Fig. 3(b) shows the ion densities

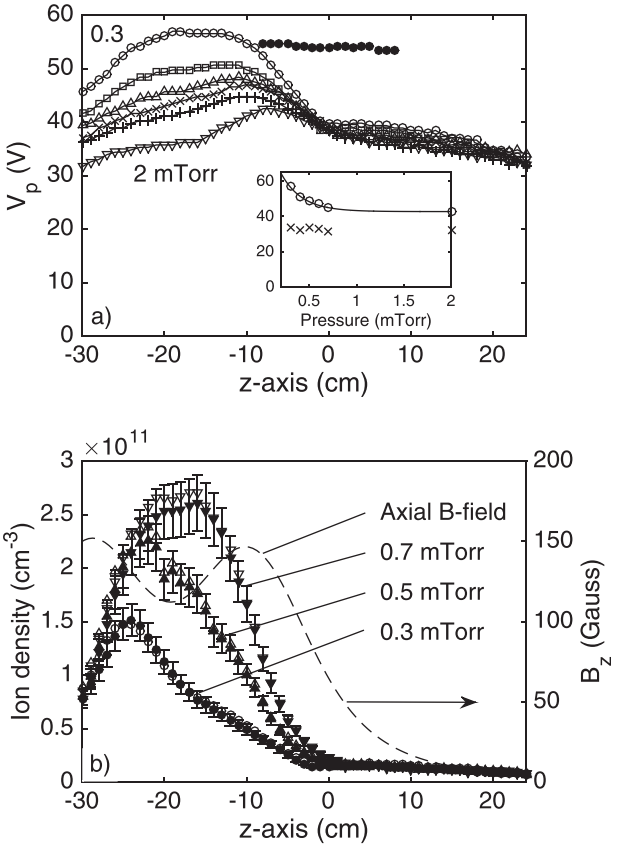

FIG. 3. Radial-facing RFEA measurements of the axial ion populations. (a) The local potential for chamber pressures of 0.3 mTorr (open circles), 0.4 mTorr (open squares), 0.5 mTorr (open upward pointing triangles), 0.6 mTorr (crosses), 0.7 mTorr (plus signs), and 2 mTorr (open downward pointing triangles). Measurements of the beam potential for 0.3 mTorr (open circles, not connected by lines) are also shown. The inset in a) shows the exponential relationship of the maximum plasma potentials with pressure (open circles and fitted exponential curve) and the invariance of the downstream plasma potential at z = 15 cm (crosses). (b) The density of the local population calculated using the drifting Maxwellians (unfilled markers) and Gaussian-flux method (filled markers) for 0.3 mTorr (circles), 0.5 mTorr (upward-pointing triangles), and 0.7 mTorr (downward-pointing triangles). The axial magnetic field profile, B_z, is also shown in b) for currents of 6 A in each solenoid.

measured by the RFEA and calculated using both methods displayed earlier for pressures of 0.3 (circles), 0.5 (upward-pointing triangles), and 0.7 mTorr (downward-pointing triangles) as well as the magnitude of the axial magnetic field, B_z (dashed curve), generated by a current of 6 A to each solenoid. The drifting Maxwellians method (unfilled markers) and Gaussian-flux method (filled markers) show strong agreement. When calculating the local ion sound speed for the Gaussian-flux method, electron temperatures of 8, 6.5, and 6 eV were used for the 0.3, 0.5, and 0.7 mTorr cases, respectively.[34] The electron temperature is known to vary axially in Chi Kung; however, a recent study showed that for the 0.3 mTorr case considered here, T_e dropped from ~9 to ~7 eV going from the source to the diffusion chamber.[18] As such, by using a T_e of 8 eV, the error in the calculated sound speed would be <10%. At a pressure of 0.3 mTorr, the profile shows a peak density of $\sim 1.5 \times 10^{11}$ cm^{-3} at z = −24 cm which then significantly decreases through the source chamber until z ~ −2 cm. Increasing the pressure to 0.7 mTorr, the peak density increases to $\sim 2.5 \times 10^{11}$ cm^{-3} and moves 8 cm downstream to z = −16 cm. It can be seen that this transition occurs as the density significantly increases in the region between z = −20 cm and z = −10 cm, immediately upstream of the throat of the magnetic nozzle. For axial positions downstream of the maximum density, the density profile can be seen to decrease with sharper gradients for increasing pressures. This change in density profile brings the maximum density closer to the outlet and moves the location of sharp density decrease downstream. This is reflected in the position of the potential drop shown in Fig. 3(a).

At the beginning of the potential drop for the 0.3 mTorr case, the Debye length is ~0.1 mm and the width of the potential drop is ~10 cm, or approximately 1000 Debye lengths. As such, the potential drops considered in this study are probably too wide to be considered strictly as double layers and can be thought of as double layer-like structures. With decreasing pressure, these would be expected to approach the classic definition of a double layer as exhibited in Ref. 7.

The source-facing RFEA is used to identify the existence of an accelerated population of ions in the measured IEDF for each test pressure and these were found for pressures of 0.7 mTorr and below. In measurements at the "start" of the expansion where the local and beam ion populations overlap, fitting to a double Gaussian can be done to extract the characteristics of each population. The beam potentials in each case are consistent with the maximum plasma potential measured upstream of the potential drop. The beam potentials for the 0.3 mTorr case are displayed in Fig. 3(a) (filled circles). Corresponding beam data for the other pressures (excluding 2 mTorr) were obtained but not shown here for clarity.

The maximum plasma potentials in each case are plotted in the inset of Fig. 3(a) and can be seen to decrease with increasing pressure. This relationship has been shown analytically and experimentally previously in Ref. 35. The inset also illustrates how the downstream plasma potentials at z = 15 cm (crosses) show little variation with pressure over this range. These trends imply that the axial potential drop is mainly dependent on the maximum potential in the source and thereby, the pressure in the system.

VI. DOWNSTREAM BEAM SPEEDS

The velocity of the ion beam measured by the source-facing RFEA can be calculated by comparing the beam and local plasma potentials at each axial location. The beam energy is simply the difference in these potentials, i.e., $E_{beam} = V_b - V_p$, where E_{beam} is the beam energy in eV. The standard equation for kinetic energy can be used to infer the velocity of ions in the beam, yielding

$$v_{beam} = \sqrt{\frac{2qE_{beam}}{M_{Ar}}}, \tag{10}$$

where v_{beam} is the beam velocity, q is the charge of an electron, and M_{Ar} is the mass of an argon ion.

Beam speeds measured with an RFEA are typically reported as a single velocity measured just downstream of the potential drop. This can be valuable for determining whether a beam is supersonic or for measuring the exhaust velocity of a thruster. Figure 4 shows the maximum downstream beam speeds measured in this study: they are shown to decrease with increasing pressure, showing consistency with the decreasing source plasma potentials shown earlier. Downstream beam speeds taken from Ref. 23 measured using the LIF techniques are also shown in the figure (solid squares) and can be seen to follow the same exponential fit. Agreement between LIF and RFEA measurements in the downstream region has previously been shown, and the present results show that this agreement is maintained during ion acceleration through the measured potential drop.

VII. BEAM ACCELERATION THROUGH POTENTIAL DROP

Reference 23 used LIF techniques to measure the increasing velocity of ions along the central axis in Chi Kung in the region of ion acceleration through the potential drop. RFEAs have typically not been used for this purpose as the presence of a large grounded probe may perturb the plasma, altering measurements of the plasma and beam potentials near the potential drop. Here a detailed investigation of the axial ion velocities in the potential drop for various pressures is carried out, and the results are compared to the previous LIF measurements in the Chi Kung reactor.

The beam velocities at each axial position can be found with Eq. (10), and Fig. 5 shows the calculated v_{beam} profiles for the same argon gas pressures as earlier. In each case, the axial beam velocity profile can be described by its behaviour in two separate regions: ion acceleration inside the potential drop and relatively constant velocity downstream.

In the region of the potential drop, the beam velocity is seen to increase sharply due to the DC axial electric field

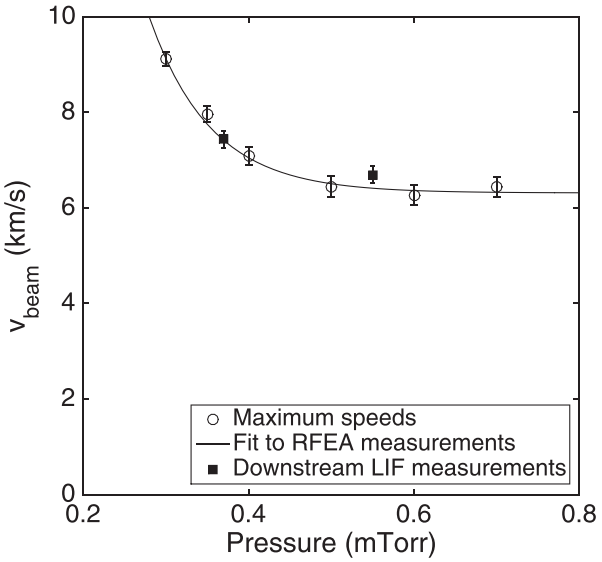

FIG. 4. Plot of the maximum beam speeds measured using the RFEA technique and Eq. (1) (open circles) with line of best fit. The LIF data from Ref. 23 are also plotted (solid squares) and can be seen to follow a similar trend with pressure.

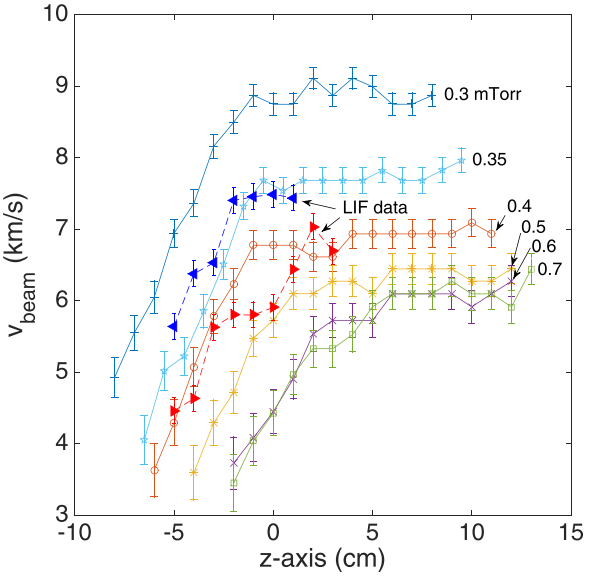

FIG. 5. Axial profiles of v_{beam} derived from the RFEA axial measurements for increasing pressures. The LIF data taken from Ref. 23 are also plotted with left-pointing (0.3 mTorr) and right-pointing (0.7 mTorr) filled triangles.

created by the potential drop. For 0.3 mTorr, the beam acceleration was detected in the region from z = −8 to −2 cm and an increase in velocity of nearly 4 km/s is observed. In this region, the gradients of the velocity profiles shown in Fig. 5 are related to the square root of the potential drop shown in Fig. 3 for each case. This explains why the gradient of the velocity profile in the higher pressure cases is reduced, i.e., ∼2 km/s over a space of 5 cm for 0.6 mTorr. The results in Fig. 3 also showed that the potential profile shifts downstream with increasing pressures, an effect that is also reflected in the locations of the acceleration in the beam velocity profiles as seen in Fig. 5.

Downstream, the velocity profiles plateau as the sharp potential drop ends. As the pressure increases, the beam velocity plateaus further downstream due to shifting of the potential profile as discussed earlier. Further, for increasing pressures, the transition between the region of ion acceleration and plateau becomes less clear as the end of the potential drop becomes less sharply defined, i.e., the DC axial electric field created by the potential drop nears that of ambipolar diffusion. The magnitudes of the downstream velocity profile also converge with increasing pressure as expected from the exponential relationships between the downstream maximum beam velocity and pressure shown in Fig. 4.

Also plotted in Fig. 5 are the beam velocities measured with LIF techniques taken from Ref. 23. The data from Ref. 23, which were measured at pressures of 0.37 mTorr and 0.55 mTorr, are limited; however, based on the limited data, the velocity profiles show good agreement of both profile shape and magnitude between RFEA and LIF results. The 0.37 mTorr LIF case, in particular, can be seen to match quite closely with an additional set of RFEA data taken at 0.35 mTorr as shown in the figure. The error bars of the LIF measurements are quoted as ±180 m/s and derived from the accuracy of the spectroscopic techniques in measuring the absolute wavelengths of an iodine cell. These error bars are

comparable to those used for the RFEA, calculated by using an uncertainty of ±0.4 V for both local and beam potentials and carrying it through Eq. (10), yielding errors that vary between approximately ±150 and ±230 m/s in the plateau region for different pressures. These results indicate that even though the RFEA is an *in situ* technique, operating in regions of high RF and DC electric fields, the ion beam velocity profiles garnered from this technique are comparable to the *ex situ* non-perturbative LIF technique. As the RFEA measurements have shown satisfactory agreement with LIF in this region, the RFEA technique can confidently be used to complete the characterisation of the beam by measuring the beam density.

VIII. BEAM DENSITY

Studying the plasma and beam densities can be interesting for propulsion applications as the momentum of ions leaving the thruster determines its performance. Previous LIF studies[19,21,23] refer to rapid metastable quenching that occurs downstream of the double layer, limiting the LIF technique's ability to probe the axial beam density. With the RFEA in ion collection mode, assumptions about metastable populations and their ability to represent the entire ion population are avoided. The I-V curves measured by the RFEA can therefore be used to calculate the axial beam density profile using the methods described earlier. The total ion density, n_{tot}, can also be inferred using $n_{tot} = n_b + n_{loc}$.[17,27] Figure 6 shows the calculated parameters for 0.3 mTorr compared to the no-beam reference case of 2 mTorr in the region where a beam is detected ($-8 \leq z \leq 8$ cm for 0.3 mTorr) for both methods of density calculation, which show satisfactory agreement. An electron temperature of 5 eV was used when calculating the ion sound speed for the 2 mTorr case.[34] It is worth noting that the Gaussian-flux method results in higher values of density than the drifting Maxwellians method for axial positions further upstream which may be due to ion transit time broadening for the higher pressure, higher plasma density case.

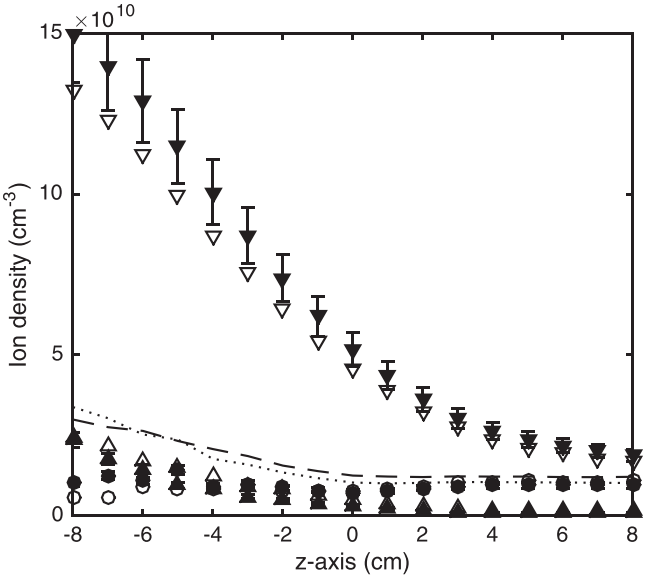

FIG. 6. Calculated values of beam density (upward-pointing triangles), local ion density (circles), and total ion density measured (lines) with the source-facing RFEA for 0.3 mTorr using the drifting Maxwellian method (unfilled markers, dashed line) and the Gaussian-flux method (filled markers, dotted line). The high pressure, no beam 2 mTorr case is also plotted (downward-pointing triangles) in the region of interest.

The total ion densities for 0.3 mTorr (lines) and 2 mTorr (downward-pointing triangles) can both be seen to follow the same expansion behaviour, i.e., reducing by a factor of ∼2 over a distance of ∼5 cm, as the magnetic field and geometric expansion are unchanged. At the beginning of the potential drop, all ions in the plasma are accelerated by the DC axial electric field, meaning that n_b and n_{tot} should be equal. As ions are accelerated, some will undergo ion-neutral charge exchange collisions, reducing the fraction of the ion population that exists in the beam. For the 0.3 mTorr case, the location at which the beam population is distinguishable from the local population ($z = -8$ cm) exhibits a beam fraction of ∼80%. This beam fraction at first detection is seen to decrease with increasing pressure as the mean free path of ion-neutral collisions subsequently shortens, i.e., ∼50% for 0.7 mTorr at $z = -4$ cm, until no beam is detected at sufficiently high pressures, e.g., the 2 mTorr case. As the beam ions travel into the expansion region, ion-neutral collisions deplete the beam population, thereby increasing the population of the local ion population. Figure 6 illustrates this for the 0.3 mTorr case where the data for n_{loc} and n_b intersect at approximately $z = -2$ cm. Further downstream, n_{loc} approaches n_{tot} as the beam becomes undetectable as a separate population in the I-V characteristic and all of the plasma exists as a stationary local population.

The ion velocity and beam results in Figs. 5 and 6 show that increasing pressure decreases the beam density fraction and velocity while increasing the total ion density at the outlet of the thruster. Previous studies have shown that maximising the total ion density at the outlet is crucial to maximising thrust[14] (and references therein), sacrificing high beam density fraction and velocity in favour of outlet density. Further, reducing the pressure to increase the magnitude of the potential drop results in diminishing returns as the velocity is dependent on the square root of this value.

IX. CONCLUSION

In this study, the velocity and density of an ion beam formed in the magnetic nozzle of a helicon double layer thruster were measured through the potential drop of a double layer-like structure for various pressures. The results showed a region of rapid acceleration coinciding with the location of the potential drop followed by a downstream velocity plateau. The highest axial beam velocity corresponds to the lowest pressure case, as expected from previous measurements. These results were compared to previous LIF measurements in the Chi Kung reactor and showed strong agreement in both profile and magnitude of velocity. As the RFEA collects all ion species, this method does not require assumptions about metastable populations and avoids the rapid quenching of these states that have been published previously and limit the ability of LIF techniques to measure the beam density through the potential drop and into the

exhaust plume. The RFEA measurements showed that the fraction of the total ion population existing as a beam was reduced with increasing pressure until, at high pressures, no beam is detected. When combined, the velocity and density results show that increasing pressure for a constant magnetic field configuration decreases the axial beam velocity but increases the ion density at the outlet of the thruster.

[1]D. M. Goebel and I. Katz, *Fundamentals of Electric Propulsion: Ion and Hall Thrusters* (John Wiley and Sons Ltd., 2008).

[2]S. Mazouffre, "Electric propulsion for satellites and spacecraft: Established technologies and novel approaches," Plasma Sources Sci. Technol. **25**(3), 033002 (2016).

[3]K. Takahashi, A. Komuro, and A. Ando, "Operating a magnetic nozzle helicon thruster with strong magnetic field," Phys. Plasmas **23**(3), 033505 (2016).

[4]L. T. Williams and M. L. R. Walker, "Thrust measurements of a radio frequency plasma source," J. Propul. Power **29**(3), 520–527 (2013).

[5]C. Charles, R. Boswell, and K. Takahashi, "Boltzmann expansion in a radiofrequency conical helicon thruster operating in xenon and argon," Appl. Phys. Lett. **102**(22), 223510 (2013).

[6]C. Charles, "A review of recent laboratory double layer," Plasma Sources Sci. Technol. **16**(4), R1–R25 (2007).

[7]C. Charles and R. Boswell, "Current-free double-layer formation in a high-density helicon discharge," Appl. Phys. Lett. **82**(9), 1356–1358 (2003).

[8]L. Conde and L. León, "Multiple double layers in a glow discharge," Phys. Plasmas **1**(8), 2441–2447 (1994).

[9]N. Plihon, P. Chabert, and C. S. Corr, "Experimental investigation of double layers in expanding plasmas," Phys. Plasmas **14**(1), 013506 (2007).

[10]I. A. Biloiu and E. E. Scime, "Temporal evolution of double layers in pulsed helicon plasmas," Appl. Phys. Lett. **95**(5), 051504 (2009).

[11]Å. Fredriksen, L. N. Mishra, and H. S. Byhring, "The effects of downstream magnetic field on current-free double layers and beam formation in the Njord helicon plasma device," Plasma Sources Sci. Technol. **19**(3), 034009 (2010).

[12]M. D. West, C. Charles, and R. W. Boswell, "Testing a helicon double layer thruster immersed in a space-simulation chamber," J. Propul. Power **24**(1), 134–141 (2008).

[13]K. Takahashi, T. Lafleur, C. Charles, P. Alexander, R. W. Boswell, M. Perren, R. Laine, S. Pottinger, V. Lappas, T. Harle, and D. Lamprou, "Direct thrust measurement of a permanent magnet helicon double layer thruster," Appl. Phys. Lett. **98**(14), 141503 (2011).

[14]T. Lafleur, K. Takahashi, C. Charles, and R. W. Boswell, "Direct thrust measurements and modelling of a radio-frequency expanding plasma thruster," Phys. Plasmas **18**(8), 080701 (2011).

[15]C. Charles, "High density conics in a magnetically expanding helicon plasma," Appl. Phys. Lett. **96**(5), 051502 (2010).

[16]K. Takahashi, C. Charles, R. Boswell, W. Cox, and R. Hatakeyama, "Transport of energetic electrons in a magnetically expanding helicon double layer plasma," Appl. Phys. Lett. **94**(19), 191503 (2009).

[17]Y. Zhang, C. Charles, and R. Boswell, "Transport of ion beam in an annular magnetically expanding helicon double layer thruster," Phys. Plasmas **21**(6), 063511 (2014).

[18]Y. Zhang, C. Charles, and R. Boswell, "Thermodynamic study on plasma expansion along a divergent magnetic field," Phys. Rev. Lett. **116**(2), 025001 (2016).

[19]S. A. Cohen, N. S. Siefert, S. Stange, R. F. Boivin, E. E. Scime, and F. M. Levinton, "Ion acceleration in plasmas emerging from a helicon-heated magnetic-mirror device," Phys. Plasmas **10**(6), 2593–2598 (2003).

[20]X. Sun, S. A. Cohen, E. E. Scime, and M. Miah, "On-axis parallel ion speeds near mechanical and magnetic apertures in a helicon plasma device," Phys. Plasmas **12**(10), 103509 (2005).

[21]X. Sun, A. M. Keesee, C. Biloiu, E. E. Scime, A. Meige, C. Charles, and R. W. Boswell, "Observations of ion-beam formation in a current-free double layer," Phys. Rev. Lett. **95**(2), 025004 (2005).

[22]C. Biloiu, X. Sun, E. Choueiri, F. Doss, E. Scime, J. Heard, R. Spektor, and D. Ventura, "Evolution of the parallel and perpendicular ion velocity distribution functions in pulsed helicon plasma sources obtained by time resolved laser induced fluorescence," Plasma Sources Sci. Technol. **14**(4), 766–776 (2005).

[23]A. M. Keesee, E. E. Scime, C. Charles, A. Meige, and R. Boswell, "The ion velocity distribution function in a current-free double layer," Phys. Plasmas **12**(9), 093502 (2005).

[24]Z. Harvey, S. C. Thakur, A. Hansen, R. Hardin, W. S. Przybysz, and E. E. Scime, "Comparison of gridded energy analyzer and laser induced fluorescence measurements of a two-component ion distribution," Rev. Sci. Instrum. **79**(10), 10F314 (2008).

[25]S. C. Thakur, A. Hansen, and E. E. Scime, "Threshold for formation of a stable double layer in an expanding helicon plasma," Plasma Sources Sci. Technol. **19**(2), 025008 (2010).

[26]N. Gulbrandsen, Å. Fredriksen, J. Carr, and E. Scime, "A comparison of ion beam measurements by retarding field energy analyzer and laser induced fluorescence in helicon plasma devices," Phys. Plasmas **22**(3), 033505 (2015).

[27]C. Charles and R. W. Boswell, "Laboratory evidence of supersonic ion beam generated by a current-free "helicon" double-layer," Phys. Plasmas **11**(4), 1706–1714 (2004).

[28]G. D. Conway, A. J. Perry, and R. W. Boswell, "Evolution of ion and electron energy distributions in pulsed helicon plasma discharges," Plasma Sources Sci. Technol. **7**(3), 337–347 (1999).

[29]C. Charles, "Hydrogen ion beam generated by a current-free double layer in a helicon plasma," Appl. Phys. Lett. **84**(3), 332–334 (2004).

[30]A. Meige, R. W. Boswell, C. Charles, and M. M. Turner, "One-dimensional particle-in-cell simulation of a current-free double layer in an expanding plasma," Phys. Plasmas **12**(5), 052317 (2005).

[31]T. E. Sheridan, "How big is a small Langmuir probe?," Phys. Plasmas **7**(7), 3084–3088 (2000).

[32]Y. Zhang, C. Charles, and R. W. Boswell, "Density measurements in low pressure, weakly magnetized, RF plasmas: Experimental verification of the sheath expansion effect," Front. Phys. **5**, 1–6 (2017).

[33]C. Charles, A. W. Degeling, T. E. Sheridan, J. H. Harris, M. A. Lieberman, and R. W. Boswell, "Absolute measurements and modeling of radio frequency electric fields using a retarding field energy analyzer," Phys. Plasmas **7**(12), 5232 (2000).

[34]K. Takahashi, C. Charles, R. W. Boswell, and T. Fujiwara, "Electron energy distribution of a current-free double layer: Druyvesteyn theory and experiments," Phys. Rev. Lett. **107**(3), 1–4 (2011).

[35]T. Lafleur, C. Charles, and R. W. Boswell, "Electron temperature characterization and power balance in a low magnetic field helicon mode," J. Phys. D: Appl. Phys. **44**(18), 185204 (2011).